

# Nonlinear Conjugate Gradient Optimization of Polyphase-Coded FM Radar Waveforms

Patrick M. McCormick and Shannon D. Blunt

Radar Systems Lab  
University of Kansas  
Lawrence, KS

**Abstract**—Polyphase-coded FM (PCFM) radar waveforms are continuous, constant amplitude, and are represented using a discrete set of parameters. This form lends itself well to descent optimization methods, with the nonlinear conjugate gradient (NLCG) method considered here. Further, a generalized integrated sidelobe (GISL) metric based on the  $q$ -norm of the autocorrelation sidelobes is introduced that includes the standard ISL and peak sidelobe level (PSL) metrics as specific cases ( $q = 2$  and  $q = \infty$ , respectively).

The notion of waveform design degrees of freedom is addressed within the context of both sampled bandwidth and 3 dB resolution bandwidth. When the sampled bandwidth is larger than the resolution bandwidth, additional degrees of freedom corresponding to the spectral roll-off region become available for use in waveform optimization. Utilizing this extra dimensionality we show that the possible optimized autocorrelation is largely independent of the waveform time-bandwidth product, which is itself defined using resolution bandwidth.

**Index Terms**—waveform design, nonlinear conjugate gradient, optimization, frequency-modulated waveforms

## I. INTRODUCTION

Frequency modulated (FM) radar waveforms have been in use for more than 50 years [1] and come in many different forms [2]–[13] (see [14], [15] for further details). Such waveforms are particularly attractive because they are inherently constant amplitude (though additional tapering may be applied) and are well-contained spectrally, thus making them amenable to implementation in high-power radar transmitters. Recently, a new form of FM waveform denoted as polyphase-coded FM (PCFM) has emerged that, along with the attractive properties above, also possesses a parameterized code-based structure that makes it suitable for the application of various optimization techniques. For example, in [16] a greedy search based on changing performance metrics (to avoid local minima) was shown to realize rather low range sidelobes relative to the waveform time-bandwidth product.

Gradient descent optimization has previously been examined (e.g. [17]–[22]) to address various attributes of radar code design. Such methods have likewise been applied to design the ambiguity function adaptively for target matched illumination [23]. To the authors’ knowledge this paper represents the first time gradient descent has been employed to design FM radar waveforms. Here, a nonlinear conjugate gradient method (NLCG) is implemented to descend iteratively on a PCFM-based performance surface that is a  $q$ -norm function of the waveform autocorrelation. Using this approach it is shown that

FM waveforms can be realized that meet the lower bound on peak sidelobe level (PSL) performance dictated by the use of a digital matched filter on receive.

Generally speaking, the determination of a radar waveform’s “goodness” is primarily determined via some measure of the properties of the waveforms autocorrelation (matched filter response) [15]. Specifically, we generally wish to minimize the sidelobes for a given mainlobe width. For  $B$  the 3 dB resolution bandwidth (associated with the matched filter resolution) and  $T$  the pulsewidth, the time-bandwidth product  $BT$  is generally viewed as a determining factor in how low these sidelobes can be driven. For example, for hyperbolic FM (HFM) waveforms the bound on PSL is  $-20\log_{10}(BT) - 3$  dB [5]. Likewise, length- $N$  Barker codes, along with their polyphase counterpart, possess the property that the PSL does not exceed  $1/N$  [14], where  $N$  also closely approximates  $BT$ .

Here we challenge this notion for FM waveforms by showing that it is actually the receiver *sampled bandwidth* that determines the sidelobe limit. For phase codes sampled once per chip interval, the resolution bandwidth and sampled bandwidth are the same. However, for FM waveforms the sampled bandwidth could be markedly higher than the resolution bandwidth. The ratio of the two is the degree of “over-sampling” with respect to the 3 dB resolution bandwidth and provides additional degrees-of-freedom for waveform design (as long as an appropriate spectral roll-off is also maintained). While such over-sampling incurs a higher computational cost for pulse compression, it is known to remediate some of the degradation that may occur from range straddling effects [24]. Further, by designing the waveform with knowledge of the degree of over-sampling, and thus the discrete length of the digital pulse compression filter, the minimum PSL for that given filter length can be achieved.

## II. PCFM WAVEFORM DEFINITION

The Polyphase-Coded FM (PCFM) waveform implementation arises from Continuous Phase Modulation (CPM) used in communications and produces continuous, constant-amplitude waveforms that are power efficient and spectrally well-contained [9]. This framework realizes FM waveforms using a discrete sequence of  $N$  parameters  $\mathbf{x} = [\alpha_1 \ \alpha_2 \ \dots \ \alpha_N]^T$  that represent piecewise instantaneous frequencies.

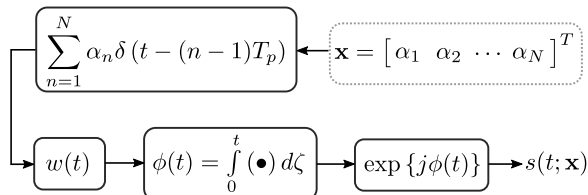


Fig. 1. Implementation of PCFM waveforms

The PCFM implementation (Fig. 1) forms a length  $N$  impulse train with time separation  $T_p$ , where the  $n$ th impulse is weighted by  $\alpha_n$ . The weighted impulse train is then filtered by the shaping filter  $w(t)$  which is typically a rectangular filter with time support on  $[0, T_p]$  that integrates to unity. The signal is then integrated to form the continuous phase signal  $\phi(t)$  defined over  $[0, T]$  for pulsewidth  $T = NT_p$ . Thus, the continuous FM waveform  $s(t; \mathbf{x})$  is

$$s(t; \mathbf{x}) = \exp \left\{ j \left( \int_0^t w(\zeta) * \sum_{n=1}^N \alpha_n \delta(\zeta - (n-1)T_p) d\zeta \right) \right\} \quad (1)$$

for  $0 < t < T$  and  $s(t; \mathbf{x}) = 0$  for  $t \notin (0, T)$ . For  $w(t)$  a rectangular filter, the phase transitions are piecewise linear. Higher-order PCFM implementations have also recently been demonstrated [11].

### III. SAMPLING, BANDWIDTH, AND PSL LOWER BOUND

The peak-normalized autocorrelation of the continuous waveform in (1) represents the matched filter response to a point scatterer and is expressed as

$$\bar{r}(\tau; \mathbf{x}) = \frac{1}{T} \int_0^T s^*(t; \mathbf{x}) s(t + \tau; \mathbf{x}) dt \quad (2)$$

for  $-T \leq \tau \leq T$ . However, when pulse compression is performed digitally, the matched filter is a sampled version of (1), where the sampling rate  $f_s = 1/T_s$  produces  $s(mT_s)$  for  $m = 1, \dots, M$  where  $M = T/T_s$  is the number of samples in the discretized waveform. Therefore, (2) becomes

$$r[\ell] = \frac{1}{M} \sum_{m=1}^M s^*(mT_s) s((m+\ell)T_s), \quad (3)$$

with  $s(mT_s) = 0$  for  $m \leq 0$  and  $m > M$ , and the dependence on  $\mathbf{x}$  is implicit. Because the discretized match filter is constant amplitude, a lower bound on the autocorrelation PSL for digital pulse compression can be defined as

$$\text{PSL}_{\text{sampled bound}} = 20 \log_{10} \left( \frac{1}{M} \right) = -20 \log_{10}(M) \quad (4)$$

which corresponds to the amplitude of  $r[\ell]$  at  $\ell = \pm(M-1)$ .

It is known that a pulsed waveform such as in (1), having finite time support on  $[0, T]$ , corresponds to a theoretically infinite bandwidth. As such, it is not theoretically possible to achieve Nyquist sampling. However, because FM waveforms such as PCFM possess good spectral containment (i.e. acceptable roll-off), the amount of aliasing can be

made small by over-sampling with respect to the 3 dB resolution bandwidth. Denote  $B = B_{\text{res}}$  as the 3 dB resolution bandwidth associated with the time-bandwidth product,  $BT$ , and  $B_{\text{samp}} = f_s = KB_{\text{res}}$  as the sampled bandwidth for over-sampling factor  $K \geq 1$ . Fig. 2 illustrates the sampled bandwidth versus the resolution bandwidth for a Gaussian power spectrum with over-sampling  $K = 3$ .

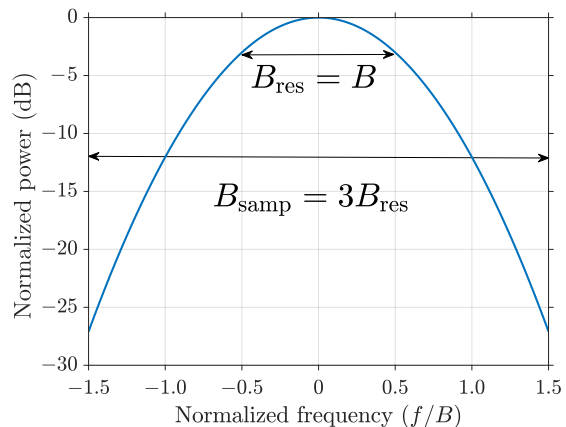


Fig. 2. Comparison of resolution bandwidth and sampled bandwidth for Gaussian power spectrum with over-sampling  $K = 3$ .

It is generally thought that the time-bandwidth product  $BT$  corresponds to the available design degrees of freedom for a waveform. However, such as was demonstrated using the notion of “over-coding” in [10], the spectral roll-off region can be used as a source of additional degrees of freedom without changing the resolution bandwidth or significantly altering the spectral containment. In that situation, the number of code values  $N$  can be made to exceed  $BT$  significantly. From a temporal perspective, this arrangement translates into finer control over the continuous transition of phase within the waveform. Use of a digital pulse compression filter means that (4) represents the lowest achievable PSL, and thus the waveform should be designed according to the  $M$  degrees of freedom available.

### IV. WAVEFORM OPTIMIZATION VIA NONLINEAR CONJUGATE GRADIENT DESCENT

The conjugate gradient method is an iterative scheme used to descend to a stationary point of some objective function that converges faster than steepest descent without requiring calculation of the Hessian [25]. The nonlinear conjugate gradient (NLCG) permits optimization of large-scale nonlinear problems as it does not require the storage of matrices. Here, the modified Hestenes-Stiefel NLCG method using a line search satisfying the strong Wolfe conditions [25] for step-size determination is implemented to optimize the vector  $\mathbf{x}$  that parameterizes the PCFM waveform.

#### A. Definition of Optimization Metric

The goodness of a given waveform is generally determined via some measure of its autocorrelation [15], with the most

well-known being PSL and ISL. Here a generalized ISL (GISL) metric is defined as a  $q$ -norm function of (2) as

$$\bar{J}_q(\mathbf{x}) = \left( \frac{2 \int_{-\Delta\tau}^T |\bar{r}(\tau)|^q d\tau}{\Delta\tau} \right)^{1/q} \quad (5)$$

where  $\Delta\tau$  is the peak-to-null width of the autocorrelation mainlobe and  $2 \leq q \leq \infty$ . The exponent  $q$  dictates the particular sidelobe metric used, with  $q = 2$  corresponding to ISL and  $q \rightarrow \infty$  to PSL. The peak-to-null mainlobe width  $\Delta\tau$  is related to the 3 dB bandwidth as  $\Delta\tau \approx 1/B$ . Using this relationship, the time-bandwidth product can be approximated using the pulse compression ratio  $T/\Delta\tau \approx BT$ .

The discretized version of (5) uses the discrete-time autocorrelation from (3) and is likewise

$$J_q(\mathbf{x}) = \left( \frac{2 \sum_{\ell=\Lambda}^{M-1} |r[\ell]|^q}{\sum_{\ell=-\Lambda+1}^{\Lambda-1} |r[\ell]|^q} \right)^{1/q}, \quad (6)$$

where  $\Lambda = \lceil f_s \Delta\tau \rceil = \lceil K \rceil$ , for  $\lceil \bullet \rceil$  the ceiling operation. Employing the relationships for pulsewidth and sampling rate realizes  $T/\Delta\tau = M/(f_s \Delta\tau) \approx M/\Lambda$ , which is used to set  $BT$  in the results that follow.

Note that the outer exponent  $(\bullet)^{1/q}$  in (5) and (6) is the reason why the general metric becomes PSL when  $q \rightarrow \infty$ . However, from a numerical standpoint very large values of  $q$  can be problematic. When more modest values are employed (e.g.  $7 \leq q \leq 10$  has been found to work well) the  $(\bullet)^{1/q}$  operation can be omitted since it does not affect the minimums in the cost function, though it is kept here for completeness. Similar metrics have also recently been used for optimization of phase codes [20], [21].

### B. Gradient Calculation

The gradient with respect to the real-valued parameter vector  $\mathbf{x}$  is composed of the partial derivatives

$$\nabla = \left[ \frac{\partial}{\partial \alpha_1} \quad \frac{\partial}{\partial \alpha_2} \quad \cdots \quad \frac{\partial}{\partial \alpha_N} \right]^T. \quad (7)$$

Application of the  $n$ th partial derivative from (7) to the cost function in (6) yields

$$\frac{\partial J_q(\mathbf{x})}{\partial \alpha_n} = \left( \frac{2 \sum_{\ell=\Lambda}^{M-1} |r[\ell]|^q}{\sum_{\ell=-\Lambda+1}^{\Lambda-1} |r[\ell]|^q} \right)^{1/q} \left[ \frac{\sum_{\ell=\Lambda}^{M-1} |r[\ell]|^q \Re \left\{ \frac{b_n[\ell] + b_n^*[-\ell]}{r[\ell]} \right\}}{\sum_{\ell=\Lambda}^{M-1} |r[\ell]|^q} - \frac{\sum_{\ell=-\Lambda+1}^{\Lambda-1} |r[\ell]|^q \Re \left\{ \frac{b_n[\ell] + b_n^*[-\ell]}{r[\ell]} \right\}}{\sum_{\ell=-\Lambda+1}^{\Lambda-1} |r[\ell]|^q} \right] \quad (8)$$

where  $\Re\{\bullet\}$  extracts the real value and

$$b_n[\ell] = \frac{-j}{M} \sum_{m=1}^M \left[ \int_0^{mT_s} w(\zeta - (n-1)T_p) d\zeta \right] s^*(mT_s) s((m+\ell)T_s). \quad (9)$$

The  $N$  partial derivatives in (8) are collected into the  $N \times 1$  gradient vector  $\nabla J_q(\mathbf{x})$  that is used in the NLCG formulation.

Note that as  $q \rightarrow \infty$ , the partial derivative in (8) reduces to the PSL form

$$\frac{\partial J_\infty(\mathbf{x})}{\partial \alpha_n} = |r[\ell_{\max}]| \Re \left\{ \frac{b_n[\ell_{\max}] + b_n^*[-\ell_{\max}]}{r[\ell_{\max}]} \right\} \quad (10)$$

where  $\ell_{\max} \in \{\Lambda, \dots, M-1\}$  is the index of the maximum sidelobe in  $r[\ell]$ . While (10) is satisfying from a completeness perspective, the gradient is discontinuous and undefined at point when two sidelobes have equal magnitude. Thus the PSL metric cannot be used in the gradient-based formulation, though it can be approximated with  $q = \text{“large”}$  (numerical issues notwithstanding).

### C. Nonlinear Conjugate Gradient Descent

The nonlinear variant of the conjugate gradient is a generalization of the linear conjugate gradient method that is known to converge faster than steepest descent while only requiring the memory storage of a few vectors. The general form of the update of vector  $\mathbf{x}_k$  at iteration  $k$  is

$$\mathbf{x}_{k+1} = \mathbf{x}_k + \mu_k \mathbf{p}_k \quad (11)$$

for direction  $\mathbf{p}_k$  and step-size  $\mu_k$ . The direction  $\mathbf{p}_k$  for NLCG is given as

$$\mathbf{p}_k = \begin{cases} \mathbf{g}_0 & \text{when } k = 0 \\ \mathbf{g}_k + \beta_k \mathbf{p}_{k-1} & \text{otherwise} \end{cases} \quad (12)$$

where  $\mathbf{g}_k = -\nabla J_q(\mathbf{x}_k)$  and  $\beta_k$  is a scalar chosen such that a conjugacy condition holds [26] (assuming exact line search). There are various adaptations to NLCG that have been proposed involving adaptation of the parameter  $\beta_k$ . Here we choose the modified Hestenes-Stiefel method of

$$\beta_k = \beta_k^{\text{HS}^+} = \max\{\beta_k^{\text{HS}}, 0\} \quad (13)$$

where

$$\beta_k^{\text{HS}} = \frac{\mathbf{g}_k^T (\mathbf{g}_k - \mathbf{g}_{k-1})}{(\mathbf{g}_k - \mathbf{g}_{k-1})^T \mathbf{p}_{k-1}} \quad (14)$$

which has a built in reset stage which reverts back to using  $\mathbf{g}_k$  when  $\beta_k^{\text{HS}} < 0$ . This method has been proven to be robust and ensure local convergence for general nonlinear cost functions that are continuously differentiable if step sizes  $\mu_k$  satisfy the strong Wolfe conditions [25], [26]. Specifically, the strong Wolfe conditions are the *sufficient decrease condition*

$$J_q(\mathbf{x}_k + \mu_k \mathbf{p}_k) \leq J_q(\mathbf{x}_k) + c_1 \mu_k \nabla J_q(\mathbf{x}_k)^T \mathbf{p}_k \quad (15)$$

and the *curvature condition*

$$\left| \nabla J_q(\mathbf{x}_k + \mu_k \mathbf{p}_k)^T \mathbf{p}_k \right| \leq c_2 \left| \nabla J_q(\mathbf{x}_k)^T \mathbf{p}_k \right| \quad (16)$$

for  $0 < c_1 < c_2 < 1$ . Here the values  $c_1 = 10^{-3}$  and  $c_2 = 0.1$  are used.

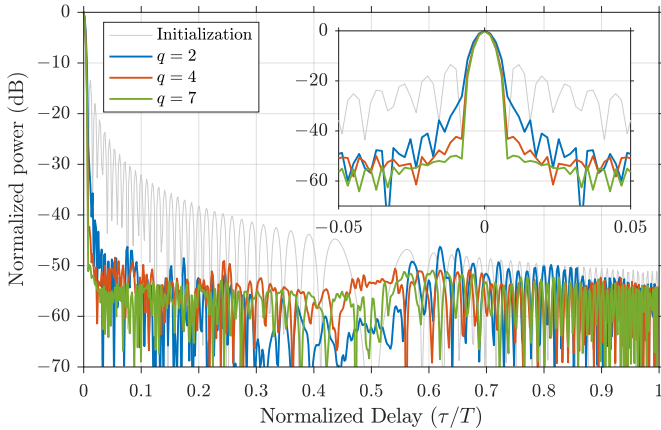


Fig. 3. Optimized PCFM autocorrelation responses of  $BT = N = 128$  and  $K = 4$  over-sampling for different  $q$ .

## V. SIMULATION RESULTS

To understand how the exponent parameter  $q$  in (6) affects the optimization, a PCFM waveform of time-bandwidth product  $BT = 128$  with over-sampling  $K = 4$  is optimized for each of the integer exponent values  $q = \{2, 4, 7\}$ . The length of the discretized waveform is  $M = 4BT = 512$ . The number of  $\alpha_n$  parameters is also set to  $N = BT = 128$ . The NLG method was initialized with the PCFM implementation of a linear-frequency modulated (LFM) waveform of the same time-bandwidth,  $BT$ .

Fig. 3 shows the converged PCFM waveform autocorrelations for  $q = \{2, 4, 7\}$ . The  $q = 2$  (ISL) case does not prioritize minimizing the energy close to the mainlobe and falls into a local minimum with relatively high PSL. Both the  $q = 4$  and  $q = 7$  cases improve on this characteristic. It was observed (though not included here) that autocorrelation responses for  $q > 7$  change only marginally from the  $q = 7$  case. For this particular initialization and set of parameters the  $q = 7$  case produced the best autocorrelation response and thus is used for the remainder of the paper.

Fig. 4 shows the autocorrelation of two optimized PCFM waveforms with  $BT = 128$  over-sampled by  $K = 4$  ( $M = 512$ ). To demonstrate how the optimization performance improves with increased degrees of freedom, the PCFM parameter vector  $\mathbf{x}$  is optimized for lengths  $N = BT = 128$  and  $N = 2BT = 256$ , where the latter represents over-coding by 2 [10]. The  $N = 256$  case has converged to a sidelobe level that is approximately 4 dB lower than the  $N = 128$  case. The doubling of the degrees of freedom has also allowed the PSL of the  $N = 256$  case, which is  $-52$  dB (near mainlobe), to get within 2.19 dB of the theoretical PSL limit of  $-54.19$  dB (from (4)). Fig. 5 shows the spectra of these two cases along with the LFM initialization of the entire sampled bandwidth. Note that by approximating  $BT \approx M/\Lambda$  we have successfully set the bandwidth  $B$  at the half-power point of the spectrum.

Now consider the case of a fixed code dimensionality of  $N = 256$  for use with a discretized matched filter length of  $M = 512$  while the time bandwidth product is varied

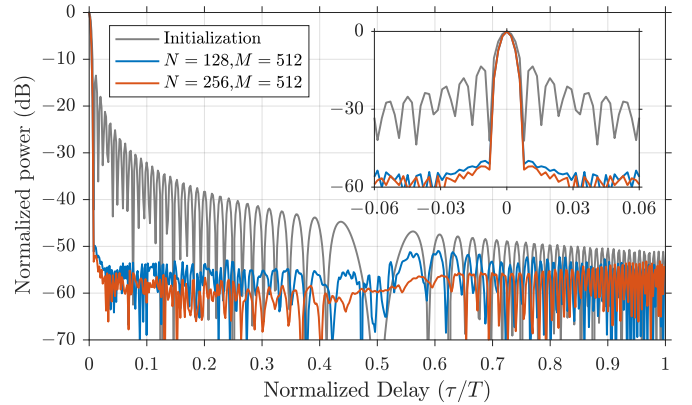


Fig. 4. Optimized PCFM autocorrelation responses using  $BT = 128$  and  $M = 4BT$  for different  $N$ .

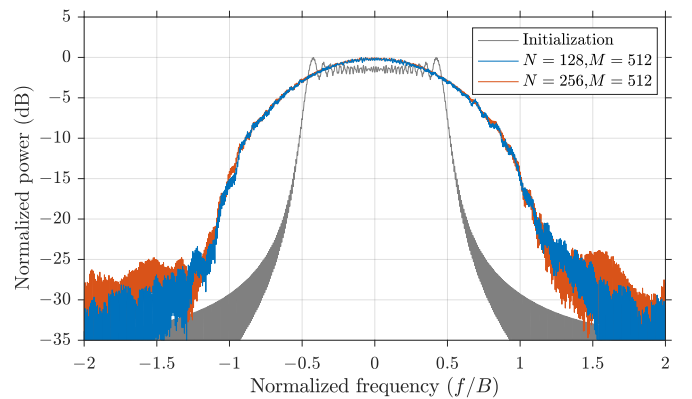


Fig. 5. Optimized PCFM power spectra using  $BT = 128$  and  $M = 4BT$  for different  $N$ .

over  $BT = \{32, 64, 128, 256\}$ . These cases correspond to respective over-coding factors of  $\{8, 4, 2, 1\}$  [10]. Likewise, the associated over-sampling factors are  $K = \{16, 8, 4, 2\}$ . It is assumed that these waveforms have the same pulsewidth  $T$ , such that a fixed  $M$  corresponds to a fixed sampled bandwidth  $B_{\text{samp}}$ . Thus the different  $BT$  values correspond to a change in the waveform resolution bandwidth  $B_{\text{res}}$ . This comparison therefore demonstrates how much of an affect  $BT$  has on the autocorrelation of an optimized waveform.

For each case, the optimization is initialized with an LFM waveform of the same  $BT$ , Fig. 6 shows the resulting power spectra after the algorithm has converged. It is interesting to note that, despite there being no explicit spectral shaping performed, each frequency response resembles a Gaussian shape which is known to correspond to low range sidelobes [4], [12], [13], [16]. Since each case has the same  $B_{\text{samp}}$ , the observed spectral content for each is dependent of the associated  $BT$ .

Fig. 7 shows the autocorrelations after convergence for the different  $BT$  cases. Notice that as  $BT$  decreases (and thus the amount of over-coding increases), the sidelobe level also decreases. The associated increase in mainlobe width and sidelobe reduction is similar to the response obtained by

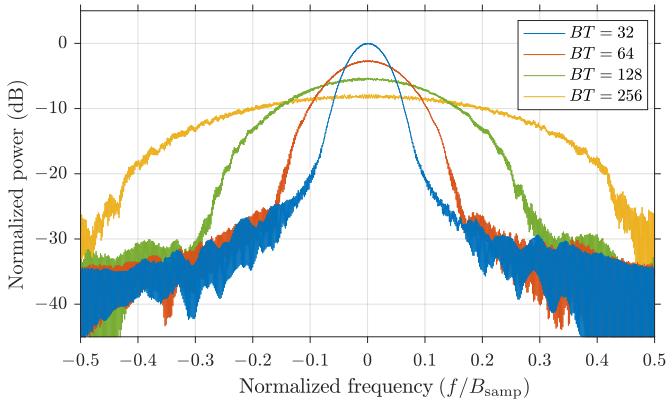


Fig. 6. Optimized PCFM power spectra for  $N = 256$  and  $M = 512$  for different  $BT$ .

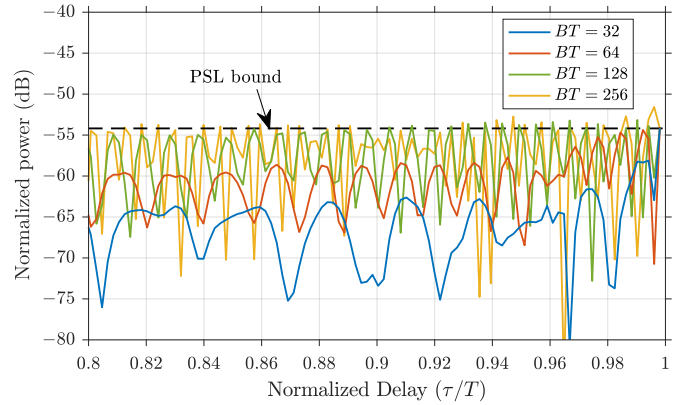


Fig. 8. Close-up optimized PCFM autocorrelation responses of  $N = 256$  and  $M = 512$  for different  $BT$ .

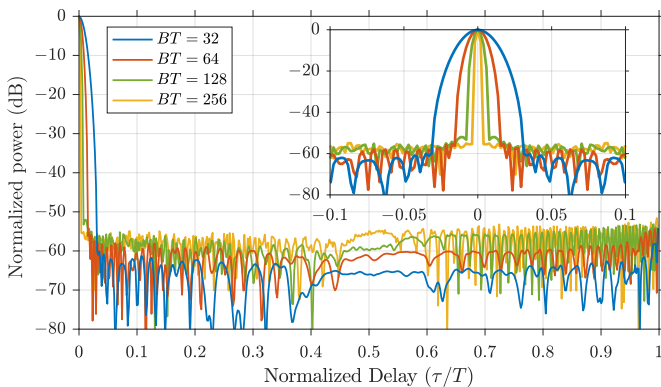


Fig. 7. Optimized PCFM autocorrelation responses for  $N = 256$  and  $M = 512$  for different  $BT$ .

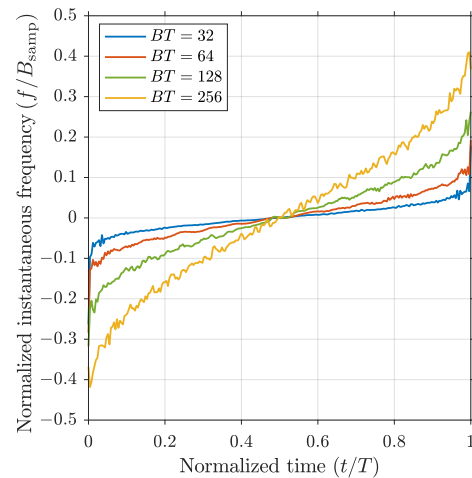


Fig. 9. Instantaneous frequency vs. time for  $N = 256$  and  $M = 512$  for different  $BT$ .

frequency tapering, albeit without the associated SNR loss. Fig. 8 provides a close-up of the outer autocorrelation values, along with the sampled PSL bound from (4) for these cases ( $-54.19$  dB). The  $BT = 128$  and  $BT = 256$  cases realize PSL values of  $-52$  dB (near mainlobe) and  $-52.74$  dB, respectively (2.19 dB and 1.45 dB above the bound). The PSL values for the  $BT = 64$  and  $BT = 32$  cases actually equals the bound at the autocorrelation edge and have much lower sidelobes at every other delay within the sidelobe region.

These examples demonstrate that it is the sampled bandwidth  $B_{\text{samp}}$  of the matched filter that determines the lower bound on PSL. Put another way, the combination of over-coding the waveform ( $N > BT$ ) and over-sampling the matched filter can facilitate substantial reductions in sidelobe levels through finer control of the spectral roll-off.

Finally, Fig. 9 shows the instantaneous time-frequency relationships for these four waveforms with different time-bandwidths. Generally speaking, each realizes the familiar “sideways-S” curve that is associated with low autocorrelation sidelobes [2]–[4]. The additional small perturbations observed in Fig. 9 are not random but arise from the optimization process (similar behavior has been observed for other FM waveform optimization approaches [9]–[11]).

## VI. CONCLUSION

The PCFM implementation is parameterized by a discrete code that characterizes the resulting continuous, constant amplitude waveform. Nonlinear conjugate gradient descent in combination with over-coding and a generalized ISL metric has been used to optimize these parameters, where it has been found that the autocorrelation of the optimized FM waveform is largely independent of the time-bandwidth product. Instead, the sampled bandwidth of the receiver matched filter dictates the achievable PSL. Further, how close one can get to this PSL bound appears to be related to the degree of waveform over-coding. Finally, this physically-realizable waveform optimization scheme is readily extensible to myriad multi-dimensional waveform-diverse radar modalities such as MIMO, pulse agility, dual-polarized, etc. [15], [27], [28].

## ACKNOWLEDGMENT

This work was supported by the Office of Naval Research under Contract # N00014-16-C-2029.

## REFERENCES

- [1] J. R. Klauder, A. C. Price, S. Darlington, and W. J. Albersheim, "The theory and design of chirp radars," *The Bell System Technical Journal*, vol. 39, no. 4, pp. 745–808, July 1960.
- [2] C. E. Cook, "A class of nonlinear FM pulse compression signals," *Proc. IEEE*, vol. 52, no. 11, pp. 1369–1371, Nov 1964.
- [3] E. Fowle, "The design of FM pulse compression signals," *IEEE Trans. Inf. Theory*, vol. 10, no. 1, pp. 61–67, Jan 1964.
- [4] J. A. Johnston and A. C. Fairhead, "Waveform design and doppler sensitivity analysis for nonlinear fm chirp pulses," *Communications, Radar and Signal Processing, IEE Proceedings F*, vol. 133, no. 2, pp. 163–175, April 1986.
- [5] T. Collins and P. Atkins, "Nonlinear frequency modulation chirps for active sonar," *IEE Proceedings - Radar, Sonar and Navigation*, vol. 146, no. 6, pp. 312–316, Dec 1999.
- [6] I. Gladkova, "Design of frequency modulated waveforms via the Zak transform," *IEEE Trans. Aerosp. Electron. Syst.*, vol. 40, no. 1, pp. 355–359, Jan 2004.
- [7] E. D. Witte and H. D. Griffiths, "Improved ultra-low range sidelobe pulse compression waveform design," *Electronics Letters*, vol. 40, no. 22, pp. 1448–1450, Oct 2004.
- [8] A. W. Doerry, *Generating nonlinear FM chirp waveforms for radar*. United States. Department of Energy, Sandia Report, SAND2006-5856, Sept. 2006.
- [9] S. D. Blunt, M. Cook, J. Jakabosky, J. D. Graaf, and E. Perrins, "Polyphase-coded FM (PCFM) radar waveforms, Part I: Implementation," *IEEE Trans. Aerosp. Electron. Syst.*, vol. 50, no. 3, pp. 2218–2229, July 2014.
- [10] J. Jakabosky, S. D. Blunt, and B. Himed, "Optimization of "over-coded" radar waveforms," in *2014 IEEE Radar Conference*, May 2014, pp. 1460–1465.
- [11] P. S. Tan, J. Jakabosky, J. M. Stiles, and S. D. Blunt, "On higher-order representations of polyphase-coded FM radar waveforms," in *2015 IEEE Radar Conference*, May 2015, pp. 467–472.
- [12] J. Jakabosky, S. D. Blunt, and T. Higgins, "Ultra-low sidelobe waveform design via spectral shaping and linc transmit architecture," in *2015 IEEE Radar Conference*, May 2015, pp. 1021–1026.
- [13] J. Jakabosky, S. D. Blunt, and B. Himed, "Spectral-shape optimized FM noise radar for pulse agility," in *2016 IEEE Radar Conference*, May 2016, pp. 1–6.
- [14] N. Levanon and E. Mozeson, *Radar signals*. John Wiley & Sons, 2004.
- [15] S. D. Blunt and E. L. Mokole, "Overview of radar waveform diversity," *IEEE Aerosp. Electron. Syst. Mag.*, vol. 31, no. 11, pp. 2–42, November 2016.
- [16] S. D. Blunt, J. Jakabosky, M. Cook, J. Stiles, S. Seguin, and E. L. Mokole, "Polyphase-coded FM (PCFM) radar waveforms, Part II: Optimization," *IEEE Transactions on Aerospace and Electronic Systems*, vol. 50, no. 3, pp. 2230–2241, July 2014.
- [17] L. K. Patton and B. D. Rigling, "Phase retrieval for radar waveform optimization," *IEEE Trans. Aerosp. Electron. Syst.*, vol. 48, no. 4, pp. 3287–3302, October 2012.
- [18] L. Li, H. Yang, G. Cui, L. Kong, and X. Yang, "Efficient phase-modulated waveform design for active sensing systems," in *2014 IEEE Radar Conference*, May 2014, pp. 1006–1009.
- [19] P. Setlur and M. Rangaswamy, "Projected gradient waveform design for fully adaptive radar STAP," in *2015 IEEE Radar Conference*, May 2015, pp. 1704–1709.
- [20] B. O'Donnell and J. M. Baden, "Fast gradient descent for multi-objective waveform design," in *2016 IEEE Radar Conference*, May 2016, pp. 1–5.
- [21] J. Song, P. Babu, and D. P. Palomar, "Sequence design to minimize the weighted integrated and peak sidelobe levels," *IEEE Trans. Signal Process.*, vol. 64, no. 8, pp. 2051–2064, April 2016.
- [22] U. Tan, C. Adnet, O. Rabaste, F. Arlery, J. P. Ovarlez, and J. P. Guyvarch, "Phase code optimization for coherent MIMO radar via a gradient descent," in *2016 IEEE Radar Conference*, May 2016, pp. 1–6.
- [23] B. J. Skinner, J. P. Donohoe, and F. M. Ingels, "Gradient descent method for designing optimum radar signals," in *Proceedings International Radar Conference*, May 1995, pp. 67–71.
- [24] D. Henke, P. McCormick, S. D. Blunt, and T. Higgins, "Practical aspects of optimal mismatch filtering and adaptive pulse compression for FM waveforms," in *2015 IEEE Radar Conference*, May 2015, pp. 1149–1155.
- [25] S. Wright and J. Nocedal, "Numerical optimization," *Springer Science*, vol. 35, 1999.
- [26] W. W. Hager and H. Zhang, "A survey of nonlinear conjugate gradient methods," *Pacific journal of Optimization*, vol. 2, no. 1, pp. 35–58, 2006.
- [27] M. Wicks and E. Mokole, *Principles of waveform diversity and design*. The Institution of Engineering and Technology, 2011.
- [28] H. Griffiths, L. Cohen, S. Watts, E. Mokole, C. Baker, M. Wicks, and S. Blunt, "Radar spectrum engineering and management: Technical and regulatory issues," *Proc. IEEE*, vol. 103, no. 1, pp. 85–102, Jan 2015.